Enantioselective oxidation of unactivated C–H bonds in cyclic amines by iterative docking-guided mutagenesis of $P450_{BM3}$ (CYP102A1)

Yuan Zhang,[1] Ziyue Xiong,[2] Yushu Li,[1] Mary Wilson,[3] Kirsten E. Christensen,[3,*] Ellie Jaques,[1] Pol Hernández-Lladó,[3] Jeremy Robertson,[2,3,*] and Luet L. Wong[1,2,*]

[1] Department of Chemistry, University of Oxford, Inorganic Chemistry Laboratory, South Parks Road, Oxford OX1 3QR, U.K.

[2] Oxford Suzhou Centre for Advanced Research, Ruo Shui Road, Suzhou Industrial Park, Jiangsu, 215123, P.R. China.

[3] Department of Chemistry, University of Oxford, Chemistry Research Laboratory, Mansfield Road, Oxford, OX1 3TA, U.K.

Corresponding authors:

Professor Luet Wong (luet.wong@chem.ox.ac.uk)

Professor Jeremy Robertson (jeremy.robertson@chem.ox.ac.uk)

Dr Kirsten Christensen (kirsten.christensen@chem.ox.ac.uk)

Abstract

Selective oxidation of ring C–H bonds is an attractive route to functionalised cyclic amines which are versatile intermediates in drug synthesis and important fragment molecules in drug discovery. Here we report a combined substrate and enzyme engineering approach to achieve enantioselective functionalisation of all unactivated C–H bonds of azepane, azocane, 7-azabicyclo[2.2.1]heptane, and 8-azaspiro[4.5]decane by cytochrome $P450_{BM3}$ (CYP102A1). Different N-modifying groups provide product diversity at high enantioselectivity (up to 99% e.e.) from a panel of just 48 variants of $P450_{BM3}$. Substrate docking into molecular dynamics simulation structures of enzyme variants is shown to be useful for designing mutations to increase enantioselectivity by disfavouring binding poses leading to the unwanted enantiomer, and to increase enzymatic activity by disfavouring non-productive poses from 10 or so variants per generation. The synthetic application of remote C–H activation within cyclic amines is exemplified by the synthesis of anisodamine via enantioselective hydroxylation of *N*-Boc-nortropinone.

Introduction

Cyclic amines have numerous applications across the chemical, agricultural and pharmaceutical industries,[1-3] for example, ~60% of U.S. FDA-approved small molecule drugs have nitrogen heterocycles in their structures.[1,4] Cyclic amines are among the most privileged core structures in this context and are crucial in fragment-based drug discovery where functionalised cyclic amine fragments provide higher hit rates.[1,3,5,6] Functionalising sp^3 C–H bonds offers a direct route to substituted cyclic amines that traditionally would be assembled by multi-step routes from acyclic precursors.[7] Current synthetic methods for these reactions have significant limitations such as the need to introduce a bespoke directing group, and difficulties in accessing unreactive C–H bonds remote from activating functionality.[8,9] Numerous reagent systems are available for α-functionalisation,[10-13] and functionalisation at

unactivated β- and γ-positions is also possible.[14-20] Nevertheless, stereoselective remote functionalisation of cyclic amines remains a challenge in synthesis. Microorganisms have been screened for cyclic amine oxidation; for example, the fungus *Beauveria bassiana* forms the β- and γ-alcohols of *N*-modified forms of 5-, 6- and 7-membered ring amines but the product selectivity cannot be controlled.[21-23]

With their mild reaction conditions and evolvable substrate specificity and product selectivity, monooxygenases, such as cytochrome P450 (CYP) enzymes, that catalyse C–H bond oxidation are attractive systems for functionalising cyclic amines. Hydroxylation of the ring carbons introduces a stereogenic centre and a synthetic handle; however, apart from drug metabolism studies,[24-26] the oxidation of cyclic amines by engineered P450 enzymes is underexplored.[27-30] P450pyr has been engineered by iterative site-saturation mutagenesis (ISM) to oxidise *N*-benzylpyrrolidine to (3*R*)- and (3*S*)-hydroxy-*N*-benzylpyrrolidine with 83% e.e. and 98% e.e., respectively.[31] $P450_{BM3}$ (CYP102A1) is the most extensively studied P450 enzyme for synthetic applications owing to its catalytic self-sufficiency and high activity.[27-30,32,33] Directed evolution of $P450_{BM3}$ by random mutagenesis, ISM and combinatorial active site saturation test coupled with high throughput screening, as well as library approaches using tens to hundreds of mutants, have expanded the substrate range and enabled the selective production of specific target compounds.[24,26,28,34-46] Molecular dynamics simulations and substrate docking have provided insight into enzyme-substrate interactions in these efforts;[37,43,46-53] however, there are few reports of the direct use of such an analysis to engineer product selectivity.[43,52,54]

Here we report a docking-guided mutagenesis approach to engineer enantioselective remote oxidation by $P450_{BM3}$ of the medium-ring amines azepane and azocane, and the bicyclic amines 7-azabicyclo[2.2.1]heptane and 8-azaspiro[4.5]decane. Initial hits were discovered by screening the amines, modified with different groups, against a library of $P450_{BM3}$ variants. Substrate docking was then used iteratively to design mutations to disfavour binding

orientations leading to the undesired enantiomer. All but one remote C–H bond of these four substrates were oxidised, the majority with >90% stereoselectivity. Application of late-stage cyclic amine functionalisation is illustrated by a stereoselective synthesis of anisodamine *via* selective hydroxylation of *N*-Boc-nortropinone by a $P450_{BM3}$ variant.

Results

$P450_{BM3}$ variant library screening and substrate engineering

The *N*-modified amine substrates were screened (0.5 mL, 1 μmol substrate) for oxidation with a panel of 48 $P450_{BM3}$ variants constructed from base variants which had been shown to have increased activity for the oxidation of a wide range of organic compounds.[55-57] Additional mutations are introduced at S72, V78, F81, A82, A184, I263, A264, E267, A328, P329, A330 and L437 (see Supplementary Figure S1).[26,44,46,58,59] The 48 selected variants (see Supplementary Table S1) contain different combinations of mutations at these residues to generate diverse binding pocket topologies. Products from preparative scale reactions (50–100 mg substrate converted) were isolated by column chromatography for characterisation.

The study began with the *N*-Boc derivatives of azepane and azocane. More than 30 of the 48 variants gave >50% conversion (total turnover number, TON ≥1000) of both *N*-Boc-azepane (**1**) and *N*-Boc-azocane (**3**) (see Supplementary Tables S3-a and S6). Oxidation at C4 (γ) dominated for both substrates; only two variants showed C3 (β) oxidation of **1** and none for **3**. The absolute configuration of 4-hydroxy-*N*-Boc-azepane, **1a**, was determined by comparison with reported specific rotation data (see Supplementary Table S12).[60] Even without optimisation, the enzyme panel achieved high enantioselectivity (Table 1 and Figure 1). The RLYF/H171L/I263G/A330W/L437S variant gave 90% of **1a** at 90% e.e. for the (*R*)-enantiomer (Table 1 and Supplementary Table S3-a) while (*S*)-**1a** was most favoured by KU3/S72W/A330P (90% of **1a** at 84% e.e.). Specific rotation data were not available for 4-hydroxy-*N*-Boc-azocane, **3a**, and Mosher ester analysis was inconclusive due to the

conformational flexibility of the 8-membered ring. Variant KU3/S72W/A330P was the most selective for the (–)-enantiomer (74% of **3a** at 77% e.e., Table 1 and Supplementary Table S6) while RLYF/I263G/A330P gave 90% of **3a** at 98% e.e. for the (+)-enantiomer. Given the similar enantioselectivity observed for each variant with *N*-modified azepane and azocane, the KU3/S72W/A330P product was assigned as the (4*S*)-alcohol and that from RLYF/I263G/A330P the (4*R*)-configuration.

More variants could easily be engineered and screened for β-oxidation of **1** and **3**, but the focus of the study moved on instead to explore the possibility of biasing the panel of 48 enzymes towards β-oxidation by changing the *N*-modifying group.[23] To this end, the *N*-Ms, *N*-Ts, *N*-Tf, and *N*-isopropylsulfonyl (*N*-Ips) derivatives of azepane and azocane were screened for oxidation. The *N*-Tf derivatives showed similar activity patterns to the *N*-Boc analogues; the *N*-Ts derivatives showed little preference for any position; the *N*-Ms derivatives gave predominantly α-oxidation (Supplementary Tables S3b – S3d). High selectivity for β-oxidation was observed for *N*-Ips-azepane (**2**) and *N*-Ips-azocane (**4**) (Table 1 and Supplementary Tables S3-a and S6). Variant VQ/S72G/A330W gave 91% of 3-hydroxy-*N*-Ips-azepane, **2b**, at 96% e.e. for (*R*)-**2b**, and R19/S72A/A330W formed 85% of 3-hydroxy-*N*-Ips-azocane, **4b**, at 99% e.e. for (*R*)-**4b**. Both (*S*)-β alcohols were most favoured by the GV/A184I/I263G/A328G variant (76% of **2b** at 79% e.e., and 76% of **4b** at 77% e.e.). The absolute configuration for (*R*)-**4b** was determined by X-ray crystallography (Figure 2 and Supplementary Table S13). Interestingly, the R19/I263G/A328L variant gave 95% of the δ-alcohol 5-hydroxy-*N*-Ips-azocane, **4a**.

Next, this approach was applied to the oxidation of 7-azabicyclo[2.2.1]heptane and 8-azaspiro[4.5]decane. Screening of the *N*-Boc, *N*-Ms, and *N*-Ips derivatives of each with the same 48-enzyme panel showed that *N*-Boc-7-azabicyclo[2.2.1]heptane, **5**, was oxidised to the *exo* (**5a**) and *endo* (**5b**) alcohols. High enantioselectivity (>90% e.e.) was observed for the *exo*

alcohols and the (*R*)-*endo* alcohol (Table 1 and Supplementary Table S12). Selectivity for the (*S*)-*endo* alcohol was lower, with GQ/I263G/A328L being the most selective one (95% of **5b** at 44% e.e.). The main goal for the spirocyclic amine was selective functionalisation of the carbocyclic ring, for which *N*-Ms-8-azaspiro[4.5]decane, **6**, furnished both the 2-alcohol **6a** and the 1-alcohol **6b**. The absolute configuration of (*S*)-**6a** was determined from the crystal structure (Figure 2 and Supplementary Table S14) and Mosher ester analysis (See Supplementary Figures S23 and S24). The variant K19/F87V/A328I gave 90% of **6a** at 88% e.e. for (*R*), and RP/H171L/I263G formed 90% of **6a** at 77% e.e. for (*S*) (Table 1 and Supplementary Table S10). The R19/F87A variant gave 96% of **6b** at 95% e.e. for (*S*) (Supplementary Table S16). No enzyme showed significant preference for the (*R*)-enantiomer of **6b**.

In summary, three *N*-modifying groups and different combinations of mutations at various residues gave remarkably enantioselective remote functionalisation of (**1**) – (**6**) by a panel of just 48 $P450_{BM3}$ variants. These enzymatic reactions are scalable; for example, the oxidation of *N*-Ips-azepane, **2** (10 mmol in 1 L), by the VQ/S72G/A330W variant (10 μmol) proceeded with 90% conversion giving (*R*)-**2b** in 80% isolated yield (1.6 g), and *N*-Boc-7-aza-bicyclo[2.2.1]heptane, **5** (6 mmol in 120 mL), was oxidised by the R19/F87I variant (0.12 μmol) with 100% conversion giving (*R*)-**5a** in 78% isolated yield (1.0 g).

Enzyme engineering by iterative docking-guided mutagenesis

Binding orientations of the modified amines in the most selective variant were modelled by computational docking to gain insight into substrate binding and to guide mutation design. Molecular dynamics (MD) simulations (100 ns) of variants in their ferryl states were carried out in triplicate. Each replica was grouped into clusters based on RMSD of Cα atoms, and the three most populated clusters were used to conduct substrate docking with Autodock Vina. The

first target was (*S*)-β oxidation of *N*-Ips-azepane (**2**), for which GV/A184I/I263G/A328G was the most selective (76% of **2b**, 79% e.e.). Docking of **2** into seven clusters across three replica simulations (See Supplementary Figures S15 and S16) showed that the lowest energy pose would give the (*S*)-β-alcohol. (*S*)-β poses were marginally the most populated productive poses (Figure 3a); however, the presence of low energy α- and γ-poses suggested a lower β-selectivity than the 76% of **2b** observed experimentally.

The (*S*)-β poses were in similar orientations within the active site model (Figure 3c). The sulfonyl oxygens of the Ips group were in van der Waals contact with G263, A264 and T268 (I helix); the isopropyl group was sequestered in a pocket formed by L75, L181, L437 and T438; while the azepane ring extended towards the β4 strand. Cβ occupied the space generated by the F87V mutation and was 3.2 Å from the ferryl oxygen but there was no direct contact with the V87 side chain. Other azepane ring carbons contacted G328, P329, T438 and the porphyrin ring. It was clear that the (*S*)-β poses would not be stable without the F87V and A328G mutations. The (*S*)-β poses were then overlaid with those indicating other products. The (*R*)-β poses were clustered together and distinct from the (*S*)-β poses, with the substrate rotated by ~90° and located closer to S72, L75 and V87 (Figure 3d). The mutations F87L/I, S72F/M and L75F/M could destabilise these (*R*)-β poses without interfering with the (*S*)-β poses, thus increasing the enantioselectivity for (*S*)-**2b**. These mutations could also disfavour some poses for α- and γ-oxidation (See Supplementary Figure S16B and S16C). It was hypothesised that enzymatic activity could potentially be improved by introducing mutations that would disfavour non-productive poses (See Supplementary Figure S16D); this hypothesis was tested with the A330F/M mutations. From this docking-guided mutagenesis approach, 10 new variants were designed.

All 10 variants showed improved selectivity or conversion (See Supplementary Table S4). The F87L variant GL/A184I/I263G/A328G showed the largest improvements, forming 94% of **2b**

at 88% e.e. The GV/A184I/I263G/A328G/A330F variant showed enhanced conversion (TON = 1350) while maintaining regioselectivity (79% of **2b**) which supported the hypothesis of increasing activity by disfavouring non-productive poses. From this, 15 variants containing two or three of these effective mutations were generated (See Supplementary Table S4). The F87L/S72F pair further improved selectivity (Figure 3e) to 96% of **2b** at 91% e.e., while F87L/A330F improved the regioselectivity and activity (97% of **2b**, 87% e.e., TON = 1450). Docking of **2** into the GL/A184I/I263G/A328G and GL/A184I/I263G/A328G/S72F variants indicated that the (*S*)-β poses were very similar to those in the GV/A184I/I263G/A328G precursor. Non-productive poses close to L188 were found that were absent in the precursor (Figure 3f). The mutations L188F/M/W were introduced to block these ~~NP~~ poses by the steric effect of their bulkier side chains. The L188F and L188W mutations nearly doubled the TON to ~900, while the variant GL/A184I/I263G/A328G/S72F/L188M gave 97% of **2b** at 92% e.e. for (*S*) with a TON of 1490 (Table 1 and Supplementary Table S4). Docking studies showed that the cluster of non-productive poses in the precursor was absent from the L188M variant (Supplementary Figure S16F). In total, 25 variants were generated in three rounds of iterative docking-guided mutagenesis (IDGM) to provide these selectivity improvements and an almost five-fold increase in TON.

Encouraged by the increases in selectivity from IDGM, the bicyclic amine **5** was docked with GQ/I263G/A328L to seek improvement of TON and 44% e.e. for the *endo*-alcohol (*S*)-**5b**. The (*R*)-*endo* and (*S*)-*endo* poses overlapped significantly (Figure 4c), which made mutation design more difficult. There were two clusters of (*S*) poses; one cluster had the Boc group oriented towards A330 and S332, and these overlapped with a group of (*R*) poses, while the Boc groups of the other cluster were closer to L75. A cluster of non-productive poses was close to A82 and T260, suggesting mutations of these two residues to increase enzymatic activity (Figure 4d). These non-productive poses were tackled first, from which it was found that the T260L

mutation raised the TON from 240 to 410; surprisingly, it also increased the enantioselectivity for (*S*)-**5b** to 76% e.e. (Table 1 and Supplementary Table S9). Mutations at A330 and S332 were then introduced to the T260L variant. The T260L/S332F combination raised the e.e. to 86% but lowered the TON. The GQ/I263G/A328L/T260L/A330F variant gave 98% of **5b** with 89% e.e. for (*S*) and higher activity (TON = 850). Two rounds of IDGM had increased the activity nearly four-fold and the enantiomeric ratio six-fold.

The IDGM approach was then applied to optimise (*S*)-β-oxidation of *N*-Ips-azocane (**4**) by GV/A184I/I263G/A328G (76% of **4b**, 77% e.e., TON = 180). Docking of **4** into this variant showed that the most populated productive poses would lead to the (*S*)-β alcohol, and the (*S*)-β poses for **2** and **4** were similar (See Supplementary Figure S19). Two rounds of IDGM led to the GV/A184I/I263G/A328G/S72F/L188F variant which gave 80% of **4b** with 91% e.e. for (*S*) (TON = 1000, Supplementary Table S7). IDGM was also successful in increasing turnover activity by disfavouring non-productive poses. The variant R19/S72A/A330W gave (*R*)-**4b** with high selectivity (85% of **4b**, 99% e.e.) but a low TON of 340. The R19/S72A/A330W/L181F variant designed from docking of **4** (See Supplementary Figures S22 and S23) showed an eight-fold improvement in TON to 2700 while maintaining the 99% e.e. (Table 1). For γ-oxidation of *N*-Boc-azepane (**1**), mutations designed from docking with the most selective variants RLYF/H171L/I263G/L437S/A330W and KU3/S72W/A330P, also increased TONs (Table 1, and see Supplementary Figures S24 – S27).

A stereoselective synthesis of anisodamine

The tropane alkaloid (3*S*,6*S*,a*S*)-anisodamine (6β-hydroxyhyoscyamine) is an anticholinergic and a1 adrenergic receptor antagonist from *Anisodus tanguticus.* This alkaloid is manufactured as a racemic mixture of diastereomers from (±)-6β-hydroxytropinone[61-63] and (±)-tropic acid for the treatment of septic shock and circulatory disorders.[64] To our knowledge, no synthesis of single anisodamine stereoisomers has been reported although relevant enantioenriched

intermediates have been prepared in multistep routes by asymmetric synthesis,[65-68] from (*R*)- or (*S*)-malic acid,[69] and by resolution.[70-72] In this context, screening of *N*-Boc-nortropinone, **7** (Figure 1), with the 48-variant library was conducted, from which 6β-alcohol **7a** was found to be the predominant product (Supplementary Table S11). Variant R19/F87A gave 95% conversion to this alcohol with 98% e.e. for the (6*R*)-enantiomer, the reaction being readily scaled to provide up to 500 mg of (6*R*)-**7a** in 70–80% isolated yield. Stereoselective reduction of the carbonyl group with L-Selectride® and further reduction, of the *N*-Boc group, afforded known diol **7c**.[73,74] Diacylated derivatives of this diol are known to be hydrolysed selectively to afford 3-acyloxy-6-hydroxytropanes;[75] reflecting this reactivity trend, monoacetylation was selective for the 6-OH leaving the 3-OH group free for further reaction. In this proof-of-principle synthesis, esterification with (±)-tropic acid and global deprotection afforded the (3*R*,6*R*,a*S*)- and (3*R*,6*R*,a*R*)- diastereomers **8a** and **8b** (*ent*-anisodamine)[76] in 15% overall yield (30 mg) from *N*-Boc-nortropinone (215 mg). The single-step enzymatic conversion of substrate **7** into (6*R*)-**7a** (76%) represents a substantial improvement on the analogous asymmetric chemical synthesis of (6*R*)-acetoxytropinone from tropinone that requires five steps (44%).[69]

Conclusion

A combination of substrate and enzyme engineering led to enantioselective oxidation, in most cases with >90% e.e., of all unactivated C–H bonds of single-ring, bridged bicyclic, and spirocyclic amines by $P450_{BM3}$ variants. The alcohol products are valuable synthetic intermediates for drugs and functionalised fragment molecules. Selectivity engineering was facilitated by the remarkably high regio- and enantio-selectivity of the screening library of 48 enzymes for the formation of almost all the alcohols. Additional mutations were designed from substrate docking to increase product selectivity by disfavouring substrate poses that led to undesired products (for example, increasing the e.e. for *S*-**5b** from 44% to 89%), and turnover activity (for example, up to eight-fold for the formation of *R*-**4b**) by disfavouring non-

productive poses. Each round of docking-guided mutagenesis required around 10 variants for significant improvements in activity and selectivity. This method of iterative docking-guided mutagenesis, which only requires the unwanted poses to be sufficiently distinct from the poses for the desired product, complements more comprehensive approaches such as random mutagenesis and ISM in engineering enzymes for application in synthesis.

Methods

The amine substrates were supplied by Fluorochem, ChemCruz, Merck and Alfa Aesar, UK. Genes encoding $P450_{BM3}$ (CYP102A1) enzymes were cloned into the pET28+ vector by NcoI and BamHI restriction sites.[55] Site-directed mutagenesis was carried out by standard PCR-based protocols using the KOD Hot Start DNA Polymerase toolkit from Sigma-Aldrich, U.K. The pET28+ plasmid harbouring the gene encoding the relevant $P450_{BM3}$ variant was transformed into *E. coli* BL21 (DE3) for enzyme production and purification. Briefly, enzyme production was induced by the addition of IPTG (0.1 mM) to *E. coli* cultures grown in $FB_{glycerol}$ and shaking for 48 h at 20 °C. Recombinant enzymes were partially purified by ammonium sulfate fractionation from the cell-free extract, firstly to 40% and then 60% saturation. The precipitated enzyme was re-dissolved in 50 mM phosphate buffer (pH 8.4) and stored at –20ºC.

Frozen stocks (10 μM) of the 48 enzymes of the screening library were thawed on ice and 50 μL of each was added to two 24-well microtitre plates which could be stored at –20 °C for at least six months. For screening experiments, the 48 enzymes in two plates were thawed to room temperature, GDH (2 U/mL), glucose (100 mM) and phosphate buffer (200 mM, pH 7.9) were added to a total volume of 0.5 mL (final enzyme concentration 1 μM). The amine substrate (200 mM stock in ethanol) was added to a final concentration of 2 mM. Reactions were initiated by the addition of $NADP^+$ (4 μM). The plates were shaken at 120 rpm for 12 h at 20 °C. Each reaction was then extracted with 0.5 mL ethyl acetate. After centrifugation at 14300 *g* to separate the phases, the organic phase was removed for analysis by GC. Preparative scale

reactions contained the same concentrations of reaction components as screening scale reactions but were conducted in larger volumes (100–500 mL). After extraction with ethyl acetate, products were separated by column chromatography, eluting with mixtures of petroleum ether and ethyl acetate.

Molecular dynamics (MD) simulations were performed on the heme domain of $P450_{BM3}$ variants in their ferryl state using the Amber 99SB*-ILDN force field with TIP3P water using GROMACS 2018.6. Mutations were added to the wild-type $P450_{BM3}$ crystal structure (PDB code: 1jpz) via Pymol. Energy minimisation, NVT and NPT equilibration steps, and production MD runs (100 ns in triplicate) were carried out using standard parameters in GROMACS.[44,46] Structures were recorded every 10 ps. Stability of the simulations was confirmed by monitoring the RMSD of the backbone Cα atoms before the individual trajectories were clustered with a cut-off of 1.2 Å. The three most populated clusters, with a population cut-off of 5% of all trajectories, were used as receptor structures for docking studies, which were performed in Autodock Vina or ADFR. All water molecules were removed from the structure prior to the docking calculation and both receptor and substrate were treated as rigid entities. In Vina, the docking site was defined as a 30 × 30 × 30 Å box centred on the ferryl oxygen, and poses were ranked using the Autodock Vina scoring function. In ADFR, the entire active site is accessible and the side chain of residues at positions 75, 78, 87, 260, 263, 267, 328, 330, 437 and 438 were selected to have full flexibility on the basis that these were most likely to contact a bound substrate.

(3*R*)-Hydroxy-*N*-Ips-azepane, 2b

A preparative scale reaction for the oxidation of *N*-Ips-azepane, **2**, to (3*R*)-hydroxy-*N*-Ips-azepane, (*R*)-**2b**, was conducted in 1 L phosphate buffer (pH 7.9, 200 mM) containing the VQ/S72G/A330W variant (10 μM), substrate **2** (2.05 g, 10 mmol added as a 200 mM stock in methanol), $NADP^+$ (4 μM), glucose (100 mM) and glucose dehydrogenase (2 U/mL). After

shaking at room temperature for 16 h, the reaction had proceeded to 90% conversion (GC). The reaction mixture was extracted with ethyl acetate (3 × 1 L). The organic extracts were combined, washed with 1 L saturated aq $NaHCO_3$ solution and then 1 L brine, dried over Na_2SO_4, filtered, and the solvent was removed by rotary evaporation. The mixture was purified by silica gel chromatography (10% ethyl acetate in petroleum ether) to give alcohol (*R*)-**2b** (96% e.e.) as a colourless oil (1.6 g, 80%).

***tert*-Butyl (1*S*,5*S*,6*R*)-6-hydroxy-3-oxo-8-azabicyclo[3.2.1]octane-8-carboxylate, 7a**

A 2000 mL conical flask was charged with phosphate buffer (pH 7.9, 200 mM, 400 mL), $NADP^+$ (5.0 mL, 5.0 mM in 200 mM phosphate buffer), glucose dehydrogenase (5.0 mL, 2.5 U/μL in 200 mM phosphate buffer), glucose (63 mL, 1.0 M in 200 mM phosphate buffer), a solution of *tert*-butyl (1*R*,5*S*)-3-oxo-8-azabicyclo[3.2.1]octane-8-carboxylate, **7** (270 mg, 1.20 mmol), in ethanol (5.0 mL), and the R19/F87A (6.0 mL, 71 μM by UV titration) variant of $P450_{BM3}$. More phosphate buffer was added until the total volume was 500 mL. The resulting solution was shaken at room temperature for 24 h then the mixture was extracted with ethyl acetate (3 × 100 mL). The combined organic extracts were washed with brine (300 mL), dried over Na_2SO_4, filtered and the solvent removed by rotary evaporation. Purification of the crude residue by silica gel chromatography (hexane/ethyl acetate, 2:1 then 1:1) gave *tert*-butyl (1*S*,5*S*,6*R*)-6-hydroxy-3-oxo-8-azabicyclo[3.2.1]octane-8-carboxylate, **7a** (220 mg, 76%), as a colourless oil.

Data Availability

All data supporting the findings of this study are available within the paper and the Supplementary Information. Source data are provided with this paper. Crystallographic data for the structures reported in this Article have been deposited at the Cambridge Crystallographic Data Centre, under deposition numbers CCDC 2159261 ((*R*)-**4b**) and

2159262 ((*S*)-**6a**). Copies of the data can be obtained free of charge via https://www.ccdc.cam.ac.uk/structures/.

Acknowledgements

This work was supported by the Biotechnology and Biological Sciences Research Council, U.K. (BB/V003445/1). Y.Z. acknowledges a University of Oxford-China Scholarship Council Graduate Scholarship. M.W. and P.H.-L. acknowledge the EPSRC Centre for Doctoral Training in Synthesis for Biology and Medicine (EP/L015838/1) for graduate studentships. For the purpose of open access, the authors have applied a creative commons attribution (CC BY) licence to any author accepted manuscript version arising.

Author Contributions

Y.Z. performed enzyme and substrate engineering, activity screening, preparative scale substrate oxidations, product characterisation, molecular dynamics simulations, substrate docking, and docking-guided mutagenesis, and wrote the paper. Z.X. performed the stereoselective synthesis of anisodamine and wrote the paper. Y.L., E.J. and P.H.-L. carried out activity screening and product characterisation experiments. M.W. performed activity screening, product characterisation and steps in the synthesis of anisodamine. K.C. determined the crystal structures to assign the absolute configurations of two products, and wrote the paper. J.R. conceived and guided the project, designed the synthesis of anisodamine, and wrote the paper. L.L.W. conceived and guided the project, designed the steps in iterative docking-guided mutagenesis, and wrote the paper.

Competing Interest Declaration

The authors declare no competing interests.

Table 1. Activity and selectivity for the oxidation of *N*-modified cyclic amines by $P450_{BM3}$ variants.
The highest selectivity from the screening panel of 48 variants and the increases obtained by iterative docking-guided mutagenesis are shown. Regio: regioselectivity; TON: total turnover number for the formation of the dominant enantiomer; NA: not applicable; –: no variant showed a preference for this enantiomer. [a] For screening scale reactions that showed 100% conversion, TON values were from reactions with higher substrate concentration and lower enzyme concentration. RLYF = R47L/Y51F; KU3 = N239H/I259V/A276T, VQ = F87V/L188Q, GV = A74G/F87V, GL = A74G/F87L, GQ = A74G/L188Q, R19 = RLYF/K19, K19 = H171L/Q307H/N319Y, RP = RLYF/I401P.

Product		Variant	Mutations	Regio.	e.e.	TON
4-Hydroxy-*N*-Boc-azepane, **1a**	(*R*)-**1a**	1	RLYF/H171L/I263G/A330W/L437S	90%	90%	10300 [a]
		2	RLYF/H171L/I263G/A330W/L437S/V78F	94%	93%	14500 [a]
	(*S*)-**1a**	3	KU3/S72W/A330P	90%	84%	8280 [a]
		4	KU3/S72W/A330P/T438F	91%	85%	12630 [a]
3-Hydroxy-*N*-Ips-azepane, **2b**	(*R*)-**2b**	5	VQ/S72G/A330W	91%	96%	1200
	(*S*)-**2b**	6	GV/A184I/I263G/A328G	76%	79%	290
		7	GL/A184I/I263G/A328G/S72F	96%	91%	480
		8	GL/A184I/I263G/A328G/S72F/L188M	97%	92%	1490
4-Hydroxy-*N*-Boc-azocane, **3a**	(*R*)-**3a**	9	RLYF/I263G/A330P	90%	98%	8910 [a]
	(*S*)-**3a**	3	KU3/S72W/A330P	74%	77%	5240 [a]
5-Hydroxy-*N*-Ips-azocane, **4a**		10	R19/I263G/A328L	95%	NA	900
3-Hydroxy-*N*-Ips-azocane, **4b**	(*R*)-**4b**	11	R19/S72A/A330W	85%	99%	340
		12	R19/S72A/A330W/L181F	84%	99%	2700
	(*S*)-**4b**	13	GV/A184I/I263G/A328G	76%	77%	180
		14	GV/A184I/I263G/A328G/S72F/L188F	80%	91%	1000
exo-2-Hydroxy-*N*-Boc-7-aza-bicyclo[2.2.1]-heptane, **5a**	(*R*)-**5a**	15	R19/F87I	99%	99%	2000
	(*S*)-**5a**	16	GL/A184I/I263G/A328G	99%	90%	2000
endo-2-Hydroxy-*N*-Boc-7-aza-bicyclo-[2.2.1]-heptane, **5b**	(*R*)-**5b**	3	KU3/S72W/A330P	89%	96%	1800
	(*S*)-**5b**	17	GQ/I263G/A328L	95%	44%	240
		18	GQ/I263G/A328L/T260L	97%	76%	410
		19	GQ/I263G/A328L/T260L/A82M	95%	79%	1070
		20	GQ/I263G/A328L/T260L/S332F	96%	86%	230
		21	GQ/I263G/A328L/T260L/S332F/A82M	94%	84%	680
		22	GQ/I263G/A328L/T260L/A330F	98%	89%	850
		23	GQ/I263G/A328L/T260L/A330F/A82M	98%	82%	900
N-Ms-8-aza-spiro[4.5]decan-2-ol, **6a**	(*R*)-**6a**	24	K19/F87V/A328I	90%	88%	1540
	(*S*)-**6a**	25	RP/H171L/I263G	90%	77%	1440
N-Ms-8-aza-spiro[4.5]decan-1-ol, **6b**	(*R*)-**6b**	–	–	–	–	–
	(*S*)-**6b**	26	R19/F87A	96%	95%	1870

Figure 1. Synthetic applications of enantioselective oxidation of cyclic amines by engineered $P450_{BM3}$.
(**a**) The oxidation products of cyclic amines modified with different protecting groups by variants of cytochrome $P450_{BM3}$. The percentages refer to regioselectivity and stereoselectivity (e.e.). The mutations in the variants are given in Table 1. (**b**) A stereoselective synthesis of anisodamine initiated by enantioselective oxidation of *N*-Boc-nortropinone. Reagents and conditions: (i) R19/F87A (0.067 mol%), 24 h, r.t.; (ii) L-Selectride, THF, –78 °C, 2 h then → r.t., 0.5 h; (iii) $LiAlH_4$, THF, 0 °C → reflux, 14 h; (iv) Ac_2O, THF, 12 h; (v) (±)-3-(*tert*-butyldimethylsilyloxy)-2-phenyl propanoic acid, DCC, DMAP, $CHCl_3$, r.t., 14 h; (vi) aq. HCl, reflux, 2.5 h then aq. NaOH (→ pH 8). (DCC: *N,N′*-dicyclohexylcarbodiimide; DMAP: 4-dimethylaminopyridine.)

Figure 2. Molecular structure of two cyclic amine oxidation products determined by single crystal X-ray diffraction.
(a) (3*R*)-Hydroxy-*N*-Ips-azocane, (*R*)-**4b**. (b) (*S*)-*N*-Ms-8-aza-spiro[4.5]decan-2-ol, (*S*)-**6a**. Thermal ellipsoids are set at 50% level. Key: nitrogen, blue; sulphur, yellow; oxygen, red; carbon, grey; hydrogen, white.

Figure 3. **Iterative docking-guided mutagenesis of $P450_{BM3}$ for the selective (*S*)-β oxidation of *N*-Ips-azepane (2).**
(**a**) The distribution of output poses and their affinity energies from the docking of **2** into clustered molecular dynamics (MD) simulation structures of the GV/A184I/I263G/A328G variant (GV = A74G/F87V). (**b**) Turnover number (TON) and e.e. for (*S*)-**2b** formation by selected variants generated in the IDGM process; blue bars are the TON for (*S*)-**2b** formation, black dots denote the regioselectivity for **2b**, red open circles denote the e.e. for (*S*)-**2b**; Precursor: GV/A184I/I263G/A328G; F87I: A74G/F87I/A184I/I263G/A328G (GI = A74G/F87I); F87L: A74G/F87L/A184I/I263G/A328G (GL = A74G/F87L); F87L/S72F: GL/A184I/I263G/A328G/S72F; F87L/S72F/L188F: GL/A184I/I263G/A328G/S72F/L188F; F87L/S72F/L188M: GL/A184I/I263G/A328G/S72F/L188M. **(c**) Overlay of (*S*)-β poses (cyan) with key active site residues (magenta) of the MD-simulated R1C1 (replica 1, cluster 1) structure of GV/A184I/I263G/A328G. (**d**) Overlay of the lowest energy (*S*)-β pose (cyan) with (*R*)-β poses (blue) from docking of **2** with GV/A184I/I263G/A328G; mutations V87L/M may destabilise these (*R*)-β poses without affecting the (*S*)-β poses and therefore improve the e.e. for (*S*)-**2b**. (**e**) Overlay of the lowest energy (*S*)-β pose (cyan) with (*R*)-β poses from docking of **2** with GL/A184I/I263G/A328G; mutations S72F/M may increase the e.e. for (*S*)-**2b**. (**f**) The lowest energy (*S*)-β pose (cyan) and non-productive poses from docking of **2** with GL/A184I/I263G/A328G/S72F; mutations L188F/M may improve enzymatic activity by lowering the population of these non-productive poses.

Figure 4. Iterative docking-guided mutagenesis for (*S*)-*endo* oxidation of *N*-Boc-7-azabicyclo[2.2.1]heptane (5).
(**a**) Distribution of output poses and their affinity energies from docking analysis of substrate **5** with the molecular dynamics simulation structure of GQ/I263G/A328L (GQ = A74G/L188Q; RxCy: simulated cluster y of replica x, numbers in brackets are the cluster sizes). **(b)** Turnover number (TON) and e.e. for *S*-**5b** of selected variants generated in the mutagenesis process; blue bars represent the TON for (*S*)-**5b**; black dots represent the regioselectivity for **5b**, red dots represent the e.e. for (*S*)-**5b**; Precursor: GQ/I263G/A328L; S332F: GQ/I263G/A328L/S332F; T260L: GQ/I263G/A328L/T260L; T260L/A82M: GQ/I263G/A328L/T260L/A82M; TL/AM/AF: GQ/I263G/A328L/T260L/A82M/A330F. (**c**) Lowest energy (*S*)-*endo* pose (cyan) overlaid with (*R*)-*endo* poses (yellow) from docking with GQ/I263G/A328L; mutations S332F/M and A330F/M are proposed to destabilise (*R*)-*endo* poses while maintaining the (*S*)-*endo* pose and improve e.e. for (*S*)-**5b**. (**d**) Lowest energy (*S*)-*endo* pose (cyan) overlaid with non-productive (NP) poses (green) from docking with GQ/I263G/A328L; mutations T260L/M and A82F/M are proposed to destabilise NP poses while maintaining the (*S*)-*endo* poses and therefore improve TON for (*S*)-**5b**.

References

1. Vitaku E., Smith D. T. & Njardarson J. T. Analysis of the structural diversity, substitution patterns, and frequency of nitrogen heterocycles among U.S. FDA approved pharmaceuticals. *J. Med. Chem.* **57**, 10257–10274 (2014).
2. Duke S. O. et al. Natural toxins for use in pest management. *Toxins* **2**, 1943–1962 (2010).
3. Murray C. W. & Rees D. C. The rise of fragment-based drug discovery. *Nat. Chem.* **1**, 187–192 (2009).
4. Taylor R. D., MacCoss M. & Lawson A. D. Rings in drugs. *J. Med. Chem.* **57**, 5845–5859 (2014).
5. Wijdeven M. A., Willemsen J. & Rutjes F. P. J. T. The 3-Hydroxypiperidine Skeleton: Key Element in Natural Product Synthesis. *Eur. J. Org. Chem.* **2010**, 2831–2844 (2010).
6. Nadin A., Hattotuwagama C. & Churcher I. Lead-oriented synthesis: a new opportunity for synthetic chemistry. *Angew. Chem. Int. Ed.* **51**, 1114–1122 (2012).
7. Vo C. V. & Bode J. W. Synthesis of saturated *N*-heterocycles. *J. Org. Chem.* **79**, 2809–2815 (2014).
8. Allwood D. M., Blakemore D. C., Brown A. D. & Ley S. V. Metal-free coupling of saturated heterocyclic sulfonylhydrazones with boronic acids. *J. Org. Chem.* **79**, 328–338 (2014).
9. Yang Y., Lan J. & You J. Oxidative C-H/C-H Coupling Reactions between Two (Hetero)arenes. *Chem. Rev.* **117**, 8787–8863 (2017).
10. Mitchell E. A., Peschiulli A., Lefevre N., Meerpoel L. & Maes B. U. Direct α-functionalization of saturated cyclic amines. *Chem. Eur. J.* **18**, 10092–10142 (2012).
11. Shaw M. H., Shurtleff V. W., Terrett J. A., Cuthbertson J. D. & MacMillan D. W. Native functionality in triple catalytic cross-coupling: sp^3 C-H bonds as latent nucleophiles. *Science* **352**, 1304–1308 (2016).
12. Chen W., Ma L., Paul A. & Seidel D. Direct α-C–H bond functionalization of unprotected cyclic amines. *Nat. Chem.* **10**, 165–169 (2018).
13. Lennox A. J. J. et al. Electrochemical Aminoxyl-Mediated α-Cyanation of Secondary Piperidines for Pharmaceutical Building Block Diversification. *J. Am. Chem. Soc.* **140**, 11227–11231 (2018).
14. Millet A., Larini P., Clot E. & Baudoin O. Ligand-controlled β-selective C(sp^3)-H arylation of *N*-Boc-piperidines. *Chem. Sci.* **4**, 2241–2247 (2013).
15. Millet A., Dailler D., Larini P. & Baudoin O. Ligand-controlled α- and β-arylation of acyclic *N*-Boc amines. *Angew. Chem. Int. Ed.* **53**, 2678–2682 (2014).
16. Topczewski J. J., Cabrera P. J., Saper N. I. & Sanford M. S. Palladium-catalysed transannular C-H functionalization of alicyclic amines. *Nature* **531**, 220–224 (2016).
17. Zhang J., Park S. & Chang S. Catalytic Access to Bridged Sila- *N*-heterocycles from Piperidines via Cascade sp^3 and sp^2 C-Si Bond Formation. *J. Am. Chem. Soc.* **140**, 13209–13213 (2018).
18. Chen W., Paul A., Abboud K. A. & Seidel D. Rapid functionalization of multiple C–H bonds in unprotected alicyclic amines. *Nat. Chem.* **12**, 545–550 (2020).
19. Oeschger R. et al. Diverse functionalization of strong alkyl C-H bonds by undirected borylation. *Science* **368**, 736–741 (2020).
20. Trindade A. F., Faulkner E. L., Leach A. G., Nelson A. & Marsden S. P. Fragment-oriented synthesis: β-elaboration of cyclic amine fragments using enecarbamates as platform intermediates. *Chem. Commun.* **56**, 8802–8805 (2020).
21. Holland H. L., Morris T. A., Nava P. J. & Zabic M. A new paradigm for biohydroxylation by *Beauveria bassiana* ATCC 7159. *Tetrahedron* **55**, 7441–7460 (1999).
22. Grogan G. J. & Holland H. L. The biocatalytic reactions of *Beauveria spp*. *J. Mol. Catal. B:Enzym.* **9**, 1–32 (2000).
23. de Raadt A., Griengl H. & Weber H. The concept of docking and protecting groups in biohydroxylation. *Chem. Eur. J.* **7**, 27–31 (2001).
24. Sawayama A. M. et al. A panel of cytochrome P450 BM3 variants to produce drug metabolites and diversify lead compounds. *Chem. Eur. J.* **15**, 11723–11729 (2009).
25. Reinen J. et al. Efficient screening of cytochrome P450 BM3 mutants for their metabolic activity and diversity toward a wide set of drug-like molecules in chemical space. *Drug Metab. Disposit.* **39**, 1568–1576 (2011).
26. Ren X. et al. Drug Oxidation by Cytochrome P450BM3 : Metabolite Synthesis and Discovering New P450 Reaction Types. *Chem. Eur. J.* **21**, 15039–15047 (2015).
27. Fasan R. Tuning P450 Enzymes as Oxidation Catalysts. *ACS Catal.* **2**, 647–666 (2012).
28. Roiban G. D. & Reetz M. T. Expanding the toolbox of organic chemists: directed evolution of P450 monooxygenases as catalysts in regio- and stereoselective oxidative hydroxylation. *Chem. Commun.* **51**, 2208–2224 (2015).
29. Wei Y., Ang E. L. & Zhao H. Recent developments in the application of P450 based biocatalysts. *Curr. Opin. Chem. Biol.* **43**, 1–7 (2018).
30. Urlacher V. B. & Girhard M. Cytochrome P450 Monooxygenases in Biotechnology and Synthetic Biology. *Trends Biotechnol.* **37**, 882–897 (2019).

31. Pham S. Q., Pompidor G., Liu J., Li X. D. & Li Z. Evolving P450pyr hydroxylase for highly enantioselective hydroxylation at non-activated carbon atom. *Chem. Commun.* **48**, 4618–4620 (2012).
32. Miura Y. & Fulco A. J. ω–1, ω–2 and ω–3 hydroxylation of long-chain fatty acids, amides and alcohols by a soluble enzyme system from *Bacillus megaterium*. *Biochim. Biophys. Acta* **388**, 305–317 (1975).
33. Whitehouse C. J. C., Bell S. G. & Wong L. L. P450BM3 (CYP102A1): connecting the dots. *Chem. Soc. Rev.* **41**, 1218–1260 (2012).
34. Glieder A., Farinas E. T. & Arnold F. H. Laboratory evolution of a soluble, self-sufficient, highly active alkane hydroxylase. *Nat. Biotechnol.* **20**, 1135–1139 (2002).
35. Reetz M. T., Bocola M., Carballeira J. D., Zha D. & Vogel A. Expanding the range of substrate acceptance of enzymes: combinatorial active-site saturation test. *Angew. Chem. Int. Ed.* **44**, 4192–4196 (2005).
36. Jung S. T., Lauchli R. & Arnold F. H. Cytochrome P450: taming a wild type enzyme. *Curr. Opin. Biotechnol.* **22**, 809–817 (2011).
37. Kille S., Zilly F. E., Acevedo J. P. & Reetz M. T. Regio- and stereoselectivity of P450-catalysed hydroxylation of steroids controlled by laboratory evolution. *Nat. Chem.* **3**, 738–743 (2011).
38. Seifert A., Antonovici M., Hauer B. & Pleiss J. An efficient route to selective bio-oxidation catalysts: an iterative approach comprising modeling, diversification, and screening, based on CYP102A1. *ChemBiochem* **12**, 1346–1351 (2011).
39. Zhang K., El Damaty S. & Fasan R. P450 fingerprinting method for rapid discovery of terpene hydroxylating P450 catalysts with diversified regioselectivity. *J. Am. Chem. Soc.* **133**, 3242–3245 (2011).
40. Zhang K., Shafer B. M., Demars M. D., 2nd, Stern H. A. & Fasan R. Controlled oxidation of remote sp^3 C-H bonds in artemisinin via P450 catalysts with fine-tuned regio- and stereoselectivity. *J. Am. Chem. Soc.* **134**, 18695–18704 (2012).
41. Narayan A. R. et al. Enzymatic hydroxylation of an unactivated methylene C-H bond guided by molecular dynamics simulations. *Nat. Chem.* **7**, 653–660 (2015).
42. Loskot S. A., Romney D. K., Arnold F. H. & Stoltz B. M. Enantioselective total synthesis of nigelladine A via late-stage C–H oxidation enabled by an engineered P450 enzyme. *J. Am. Chem. Soc.* **139**, 10196–10199 (2017).
43. Acevedo-Rocha C. G. et al. P450-Catalyzed Regio- and Diastereoselective Steroid Hydroxylation: Efficient Directed Evolution Enabled by Mutability Landscaping. *ACS Catal.* **8**, 3395–3410 (2018).
44. Li Y. & Wong L. L. Multi-Functional Oxidase Activity of CYP102A1 (P450BM3) in the Oxidation of Quinolines and Tetrahydroquinolines. *Angew. Chem. Int. Ed.* **58**, 9551–9555 (2019).
45. Li A. et al. Regio- and Stereoselective Steroid Hydroxylation at the C7-Position by Cytochrome P450 Monooxygenase Mutants. *Angew. Chem. Int. Ed.* **59**, 12499–12505 (2020).
46. Chen W., Fisher M. J., Leung A., Cao Y. & Wong L. L. Oxidative Diversification of Steroids by Nature-Inspired Scanning Glycine Mutagenesis of P450BM3 (CYP102A1). *ACS Catal.* **10**, 8334–8343 (2020).
47. Paulsen M. D. & Ornstein R. L. Dramatic differences in the motions of the mouth of open and closed cytochrome P450BM3 by molecular dynamics simulations. *Proteins: Struct., Funct., Genet.* **21**, 237–243 (1995).
48. Pleiss J. Systematic Analysis of Large Enzyme Families: Identification of Specificity- and Selectivity-Determining Hotspots. *ChemCatChem* **6**, 944–950 (2014).
49. Dodani S. C. et al. Discovery of a regioselectivity switch in nitrating P450s guided by molecular dynamics simulations and Markov models. *Nat. Chem.* **8**, 419–425 (2016).
50. Capoferri L. et al. Insights into regioselective metabolism of mefenamic acid by cytochrome P450 BM3 mutants through crystallography, docking, molecular dynamics, and free energy calculations. *Proteins: Struct., Funct., Bioinf.* **84**, 383–396 (2016).
51. Ebert M. C. C. J. C., Espinola J. G., Lamoureux G. & Pelletier J. N. Substrate-Specific Screening for Mutational Hotspots Using Biased Molecular Dynamics Simulations. *ACS Catal.* **7**, 6786–6797 (2017).
52. Petrovic D., Bokel A., Allan M., Urlacher V. B. & Strodel B. Simulation-Guided Design of Cytochrome P450 for Chemo- and Regioselective Macrocyclic Oxidation. *J. Chem. Inf. Model.* **58**, 848–858 (2018).
53. Li Z. et al. Engineering cytochrome P450 enzyme systems for biomedical and biotechnological applications. *J. Biol. Chem.* **295**, 833–849 (2020).
54. Peng Y. Q. et al. A Chemoenzymatic Strategy for the Synthesis of Steroid Drugs Enabled by P450 Monooxygenase-Mediated Steroidal Core Modification. *ACS Catal.* **12**, 2907–2914 (2022).
55. Whitehouse C. J. C. et al. Evolved CYP102A1 (P450BM3) variants oxidise a range of non-natural substrates and offer new selectivity options. *Chem. Commun.*, 966–968 (2008).
56. Whitehouse C. J. C. et al. Structural basis for the properties of two single-site proline mutants of CYP102A1 (P450BM3). *ChemBiochem* **11**, 2549–2556 (2010).
57. Whitehouse C. J. C. et al. Structure, Electronic Properties and Catalytic Behaviour of an Activity-Enhancing CYP102A1 (P450BM3) variant. *Dalton Trans.* **40**, 10383–10396 (2011).

58. Ren X., O'Hanlon J. A., Morris M., Robertson J. & Wong L. L. Synthesis of Imidazolidin-4-ones via a Cytochrome P450-Catalyzed Intramolecular C–H Amination. *ACS Catal.* **6**, 6833–6837 (2016).
59. O'Hanlon J. A., Ren X., Morris M., Wong L. L. & Robertson J. Hydroxylation of anilides by engineered cytochrome P450BM3. *Org. Biomol. Chem.* **15**, 8780–8787 (2017).
60. Li C., Liu Y., Pei X.-Q. & Wu Z.-L. Stereo-complementary bioreduction of saturated *N*-heterocyclic ketones. *Process Biochem.* **56**, 90–97 (2017).
61. Sheehan J. C. & Bloom B. M. The Synthesis of Teloidinone and 6-Hydroxytropinone. *J. Am. Chem. Soc.* **74**, 3825–3828 (1952).
62. Stoll A., Becker B. & Jucker E. Synthesis of α-hydroxysuccinaldehyde and 3,6-dihydroxytropane. *Helv. Chim. Acta* **35**, 1263–1269 (1952).
63. Nedenskov P. & Clauson-Kaas N. Simplified Preparation of 6-Hydroxytropinone. *Acta Chem. Scand.* **8**, 1295–1295 (1954).
64. Yu Y. T. et al. Effectiveness of anisodamine for the treatment of critically ill patients with septic shock: a multicentre randomized controlled trial. *Crit. Care* **25**, 349 (2021).
65. Majewski M. & Lazny R. Stereoselective synthesis of tropane alkaloids: Physoperuvine and dihydroxytropanes. *Synlett*, 785–786 (1996).
66. Majewski M., Lazny R. & Ulaczyk A. Enantioselective ring opening of tropinone. A new entry into tropane alkaloids. *Can. J. Chem.* **75**, 754–761 (1997).
67. Cramer N., Laschat S., Baro A. & Frey W. Enantioselective desymmetrization of tropinone derivatives by hydroboration. *Synlett*, 2175–2177 (2003).
68. Kulkarni K., Zhao A. Y., Purcell A. W. & Perlmutter P. The enantioselective total synthesis and unambiguous proof of the absolute stereochemistry of pervilleine C. *Synlett*, 2209–2212 (2008).
69. Mao Z. Y., Huang S. Y., Gao L. H., Wang A. E. & Huang P. Q. A novel and versatile method for the enantioselective syntheses of tropane alkaloids. *Sci. China Chem.* **57**, 252–264 (2014).
70. Fodor G. & Kovacs O. The Stereochemistry of the Tropane Alkaloids .3. The Configuration of Scopolamine and of Valeroidine. *J. Chem. Soc.*, 2341–2344 (1953).
71. Cramer N., Laschat S. & Baro A. Enzymatic resolution of tropinone derivatives. *Synlett*, 2178–2181 (2003).
72. Niu Y. Y. et al. The absolute configuration plays an important role in muscarinic activity of BGT-A and its analogs. *Bioorgan. Med. Chem.* **16**, 10251–10256 (2008).
73. Fodor G. & Soti F. Correlation of valeroidine with S-(–)-methoxysuccinic acid and of mono-tigloyltropane and ditigloyltropane-3.6-diol with Its R-(+)-antimer. *Tetrahedron Lett.*, 1917–1921 (1964).
74. Munoz M. A., Munoz O. & Joseph-Nathan P. Absolute configuration determination and conformational analysis of (–)-(3*S*,6*S*)-3α,6β-diacetoxytropane using vibrational circular dichroism and DFT techniques. *Chirality* **22**, 234–241 (2010).
75. Fodor G., Toth J. & Vincze I. W. Stereochemistry of tropane alkaloids. 13. Absolute configuration and a simplified syntheses of valeroidine. *J. Chem. Soc.*, 3219–3221 (1961).
76. Wu T. et al. Preparative separation of four isomers of synthetic anisodamine by HPLC and diastereomer crystallization. *Chirality* **31**, 11–20 (2019).

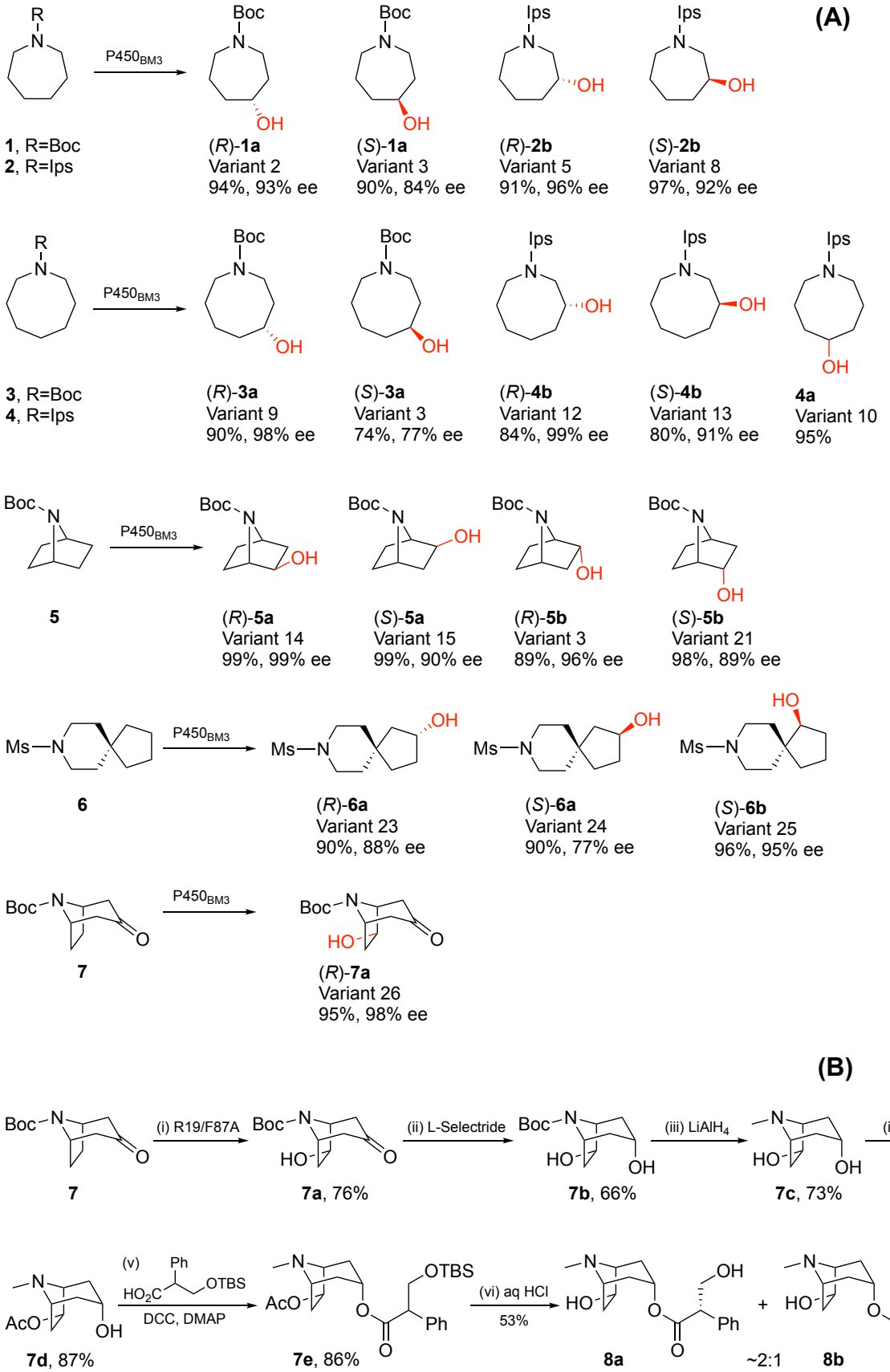
(A)
P450BM3
1, R=Boc
2, R=Ips
(R)-1a
Variant 2
94%, 93% ee
(S)-1a
Variant 3
90%, 84% ee
(R)-2b
Variant 5
91%, 96% ee
(S)-2b
Variant 8
97%, 92% ee
3, R=Boc
4, R=Ips
(R)-3a
Variant 9
90%, 98% ee
(S)-3a
Variant 3
74%, 77% ee
(R)-4b
Variant 12
84%, 99% ee
(S)-4b
Variant 13
80%, 91% ee
4a
Variant 10
95%
5
(R)-5a
Variant 14
99%, 99% ee
(S)-5a
Variant 15
99%, 90% ee
(R)-5b
Variant 3
89%, 96% ee
(S)-5b
Variant 21
98%, 89% ee
6
(R)-6a
Variant 23
90%, 88% ee
(S)-6a
Variant 24
90%, 77% ee
(S)-6b
Variant 25
96%, 95% ee
7
(R)-7a
Variant 26
95%, 98% ee
(B)
(i) R19/F87A
(ii) L-Selectride
(iii) LiAlH4
(iv) Ac2O
7
7a, 76%
7b, 66%
7c, 73%
7d, 87%
(v)
DCC, DMAP
7e, 86%
(vi) aq HCl
53%
8a
~2:1
8b

Figure 1

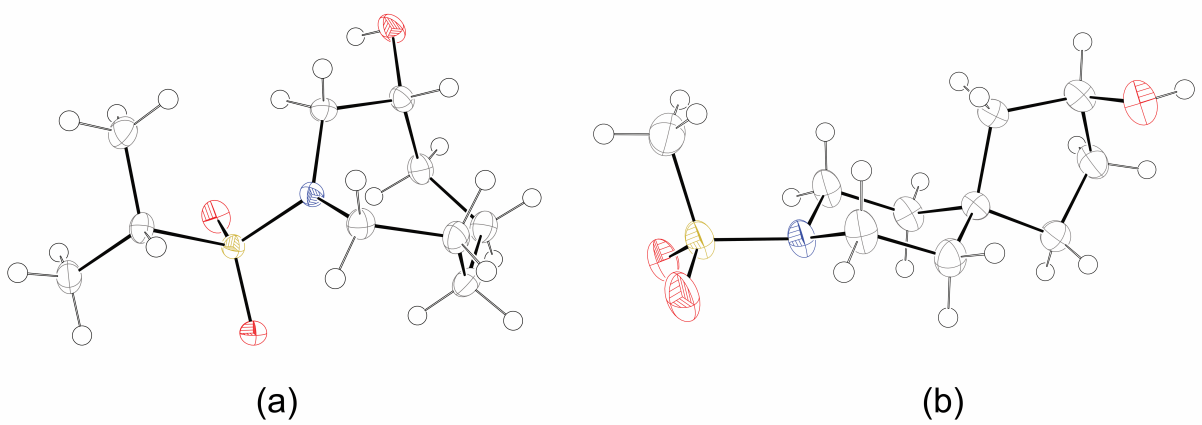

Figure 2

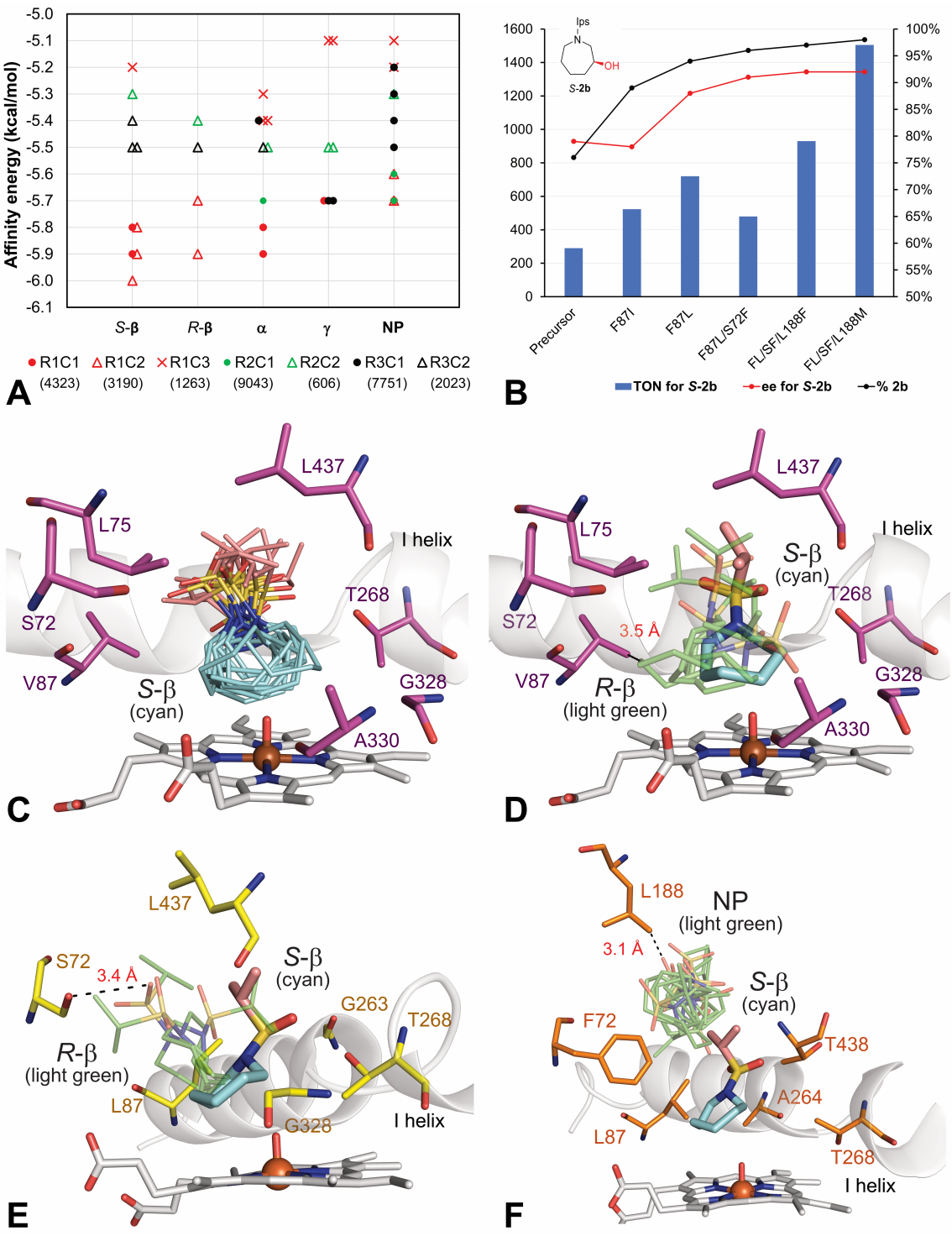
A
Affinity energy (kcal/mol)
-5.0
-5.1
-5.2
-5.3
-5.4
-5.5
-5.6
-5.7
-5.8
-5.9
-6.0
-6.1
S-β
R-β
α
γ
NP
R1C1 (4323)
R1C2 (3190)
R1C3 (1263)
R2C1 (9043)
R2C2 (606)
R3C1 (7751)
R3C2 (2023)
B
Ips
OH
S-2b
1600
1400
1200
1000
800
600
400
200
0
100%
95%
90%
85%
80%
75%
70%
65%
60%
55%
50%
Precursor
F87I
F87L
F87L/S72F
FL/SF/L188F
FL/SF/L188M
TON for S-2b
ee for S-2b
% 2b
C
L437
L75
I helix
T268
S72
V87
S-β
(cyan)
G328
A330
D
L437
L75
I helix
S-β
(cyan)
T268
S72
3.5 Å
V87
R-β
(light green)
G328
A330
E
L437
S72
3.4 Å
S-β
(cyan)
G263
T268
R-β
(light green)
L87
G328
I helix
F
L188
NP
(light green)
3.1 Å
S-β
(cyan)
F72
T438
A264
L87
T268
I helix

Figure 3

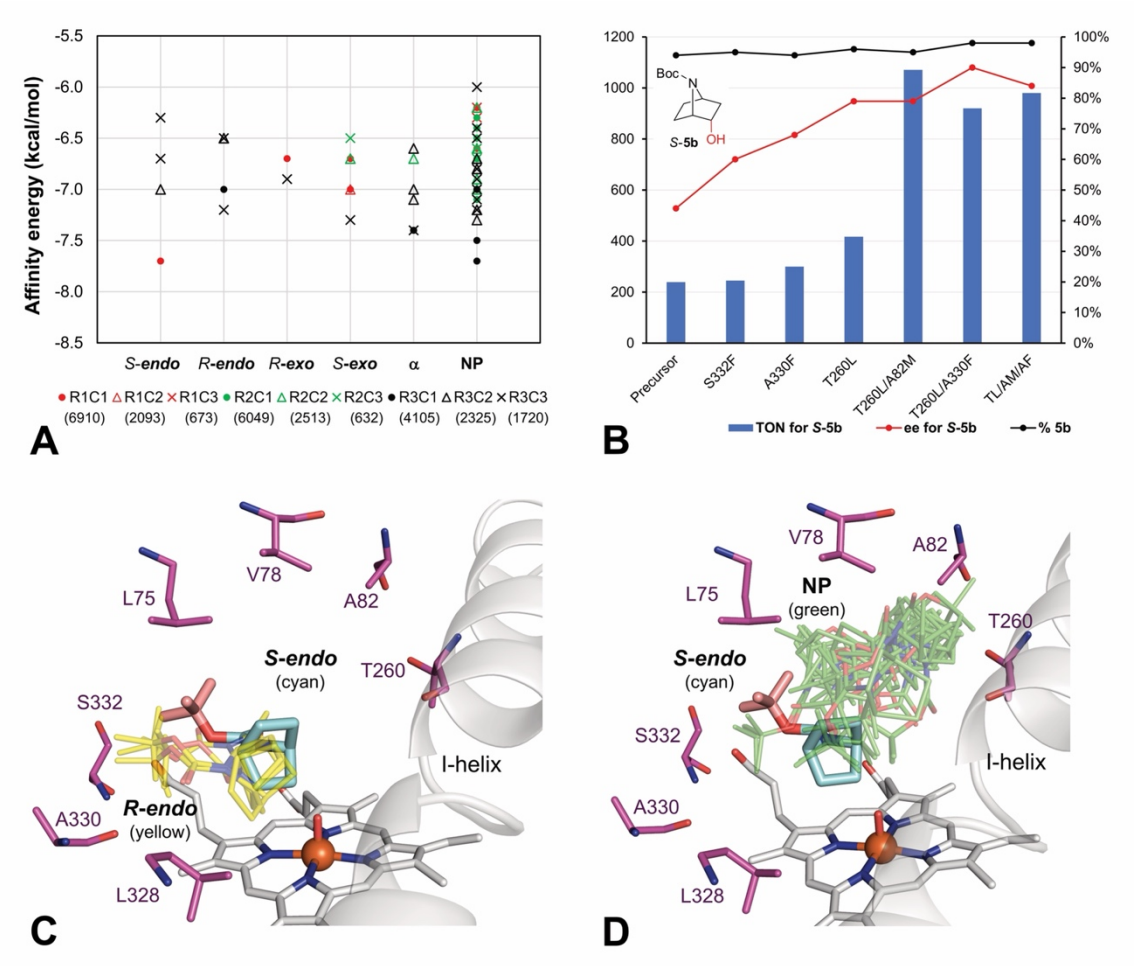
Affinity energy (kcal/mol)
-5.5
-6.0
-6.5
-7.0
-7.5
-8.0
-8.5
S-endo
R-endo
R-exo
S-exo
α
NP
R1C1 R1C2 R1C3 R2C1 R2C2 R2C3 R3C1 R3C2 R3C3
(6910) (2093) (673) (6049) (2513) (632) (4105) (2325) (1720)
A
1200
1000
800
600
400
200
0
100%
90%
80%
70%
60%
50%
40%
30%
20%
10%
0%
Boc
N
S-5b
OH
Precursor
S332F
A330F
T260L
T260L/A82M
T260L/A330F
TL/AM/AF
TON for S-5b
ee for S-5b
% 5b
B
L75
V78
A82
S-endo
(cyan)
T260
S332
I-helix
R-endo
(yellow)
A330
L328
C
V78
A82
L75
NP
(green)
T260
S-endo
(cyan)
S332
I-helix
A330
L328
D

Figure 4